De novo design of proteins that bind naphthalenediimides, powerful photooxidants with tunable photophysical properties

Samuel I. Mann[‡§†], Zhi Lin[‡], Sophia K. Tan[‡§], Jiaqi Zhu, Zachary X. W. Widel, Ian Bakanas[‡§], Jarrett P. Mansergh, Rui Liu[¶††], Mark J. S. Kelly[‡], Yibing Wu[‡*], James A. Wells[*,‡,||], Michael J. Therien[*¶], and William F. DeGrado[*,‡,§]

[‡]Department of Pharmaceutical Chemistry, University of California at San Francisco, San Francisco, California 94158-9001, United States

[§]The Cardiovascular Research Institute, University of California at San Francisco, San Francisco, California 94158-9001, United States

[||]Department of Cellular and Molecular Pharmacology, University of California, San Francisco, San Francisco, CA 94158, USA

[¶]Department of Chemistry, Duke University, Durham, North Carolina 27708, United States

ABSTRACT: *De novo* protein design provides a framework to test our understanding of protein function. Ligand binding, while simple in concept, is an ongoing challenge requiring precise placement of polar groups within a protein core. Addressing this challenge enables binding of abiological cofactors with interesting chemical properties. Here, we report the design of a helical bundle to bind naphthalenediimides (NDIs), powerful photooxidants with tunable photophysical properties. We augmented our design methods with MD simulations to assess dynamics within the binding site, including four H-bonding interactions to the NDI carbonyls. The MD simulations were validated by solution NMR which showed a helical backbone with 0.9 Å rmsd relative to the design and 19 NOEs between the NDI and the protein. We utilize two NDI cofactors in this *de novo* protein and use ultra-fast pump-probe spectroscopy to demonstrate light-triggered intra- and intermolecular electron transfer function. Moreover, we highlight the utility of this platform to activate molecular probes for protein proximity labeling in a light dependent manner.

INTRODUCTION

In nature, proteins bind a diverse array of small molecules to accomplish organismal function from light-harvesting to cellular signaling. These proteins have evolved to recognize molecular shape and electron density distribution, enabling them to bind specific molecules within the complex biological milieu. The design of small molecule-binding proteins is an ongoing challenge for the protein design community. The problem has been described as that of "inverse drug design", where atomic-level positioning of amino acid side chains and ligand are required for high affinity binding.[1] Solving this challenge could enable the design of proteins that bind new-to-nature cofactors which leverage the advantages of proteins (genetically encodable, evolvable, expressible) with chemical properties that enable catalysis, photophysics, and photochemistry not found in nature. Biological photocatalysis (outside of the photosynthetic pathway) is limited to flavoproteins that use flavin adenine dinucleotide (FAD) or flavin mononucleotide (FMN). While they perform important functions in nature, they are far too expensive for industrial processes. Moreover, the limited options for biological photocatalysts contrasts with the widespread use of photocatalysis in chemical synthesis and in applications that include the production of solar fuels.[2-3] Alternatively, could we design enzymes for new-to-nature photoredox catalysis using fully *de novo* proteins and inexpensive organic photooxidants? Here, we take important first steps towards this goal.

Recent advancements in design methodology, particularly spurred by advances in machine learning, have enabled the design of proteins that bind organic small molecules and cofactors tightly (low nM to pM).[4-9] However, until recently, the few successful examples of nM binders have depended on screening of a large library of designs or high-throughput evolution methods[4-5, 10-12] and have been focused on those close to nature or with known binding sites in the PDB[4-5, 9]. Attempts to design binding sites using *de novo* protein pseudo-cycles led to proteins with approximately 0.1 μM to 10 μM (prior to optimization) binding affinity for FITC-conjugated ligands. Therefore, the ability to design binders for fully non-natural cofactors is a challenge that must be addressed. In this work, we describe the *de novo* design of a helical bundle protein that binds naphthalenediimides (NDIs, Fig. 1), abiological photooxidants not seen in proteins, with high affinity.

NDIs (Fig. 1A) are a well-studied class of molecules with unique electronic structural and photophysical properties that may be precisely modulated via established and straightforward synthetic methods.[13-14] Their stability has led to their use in multiple functional materials[15], DNA intercalation[16], and electron donor-acceptor (DA) systems[17-18]. In addition, NDIs are powerful photooxidants; for example, an NDI bearing no bay region (naphthyl framework) substituents features a singlet excited state reduction potential ($^1E^{-/*}$) > 2.40 V (vs SCE),[19] and is thus capable of oxidizing aromatic amino acids Phe, Tyr, and Trp (Fig. 1B) via a photoinduced hole transfer reaction.[20] Combined with the ability to tune their electronic properties through substituent effects and H-bonding interactions, NDIs are enticing targets for protein design where they have potential as powerful photocatalysts[21] or photosensitizers.[13-14, 22-24] We initially focused on NDI derivative NDI-**1** (Fig 1B) due to its ability to perform intramolecular charge transfer[19] (Fig. 1A) and its relevance in synthetic donor-acceptor (DA) systems that include a de novo protein design that bound a covalently linked NDI-metalloporphyrin moiety.[13, 25] Following photoexcitation, NDI**1** undergoes intramolecular ET (lifetime of charge-separated state (CS) ~ 1 ps, Fig. 1A)[19]. Alkyl-substituted NDI**2** (Fig. 1B), incapable of undergoing photoinduced intramolecular ET, can trigger a variety of intermolecular ET reactions that include oxidizing nearby residues and forming CS states with lifetimes on the order of ns (Fig. 1A).[26] Tight binding and precise positioning of NDI cofactors within a designed protein would enable diverse strategies for manipulation of ET dynamics and realization of complex photo-oxidative function.[27]

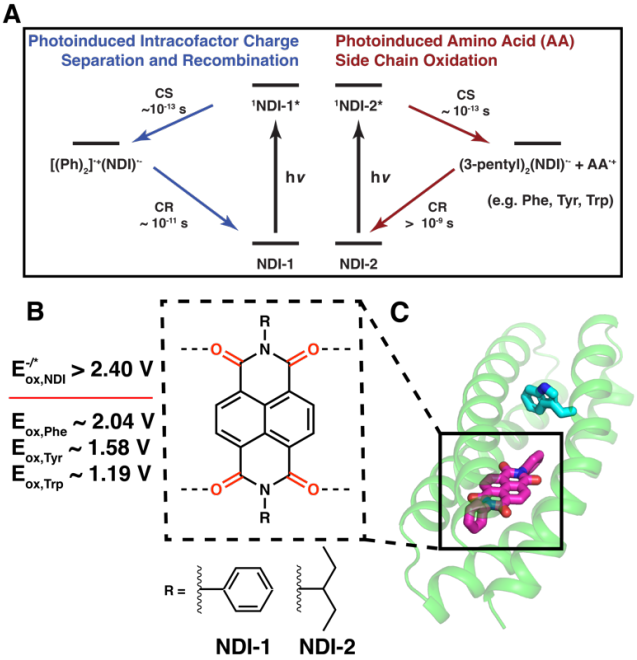

Figure 1. (**A**) Jablonski diagram illustrating photoinduced intramolecular CS/CR (left) and intermolecular CS/CR (right) reactions that may be triggered by an electronically excited NDI**1** or NDI2 (^{1}NDI*) cofactor. (**B**) NDI cofactors for intramolecular (NDI**1**) and intermolecular (NDI**2**) photoinduced charge separation reactions. (**C**) General model of an NDI-binding protein used in this study with binding site that includes H-bonds to the carbonyl oxygens (dashed lines). Potentials shown are relative to the SCE reference electrode.

The design of diverse binders necessitates an ability to accommodate polar functional groups; in this regard, hydrogen bonds (H-bonds) provide keystone interactions with NDI carbonyl moieties as well as define a powerful tool to regulate the redox potential of these bound cofactors. A challenge stems from the fact that polar groups on a ligand such as NDI must lose their favorable interactions with water molecules upon binding to the protein. To offset this, polar protein side chains must establish precise polar interactions (such as H-bonds) with the bound cofactor.

We recently showed that helical bundles can be designed to bind polar ligands, such as the drugs apixaban[5] or rucaparib[4], with high affinity using COMBS (Convergent Motifs for Binding Sites). This computational method utilizes van der Mers (vdMs) to sample protein functional group (FG) interactions throughout the PDB. Each FG on a ligand of interest is approximated with a common protein FG (i.e., amide, carbonyl, or hydroxyl) and sampled against this database of protein structures. Sampling of these interactions allows us to spatially position FGs on a ligand relative to the backbone atoms of an amino acid sidechain. The COMBS algorithm then finds multiple positions on a given protein scaffold that can form favorable H-bonding interactions with the FGs on a target molecule, constructing a custom binding site and superposing the ligand into an ideal pose.[5]

These accomplishments illustrated advances in design methods that include polar ligand binding sites and as well as a physical (rather than purely statistical) approach to cofactor binding. In these previous cases, however, existing structures of ligand-protein complexes helped inform the design process, but here we test the generalizability of our approach on a fully abiological photooxidant that does not appear in nature. Furthermore, we augment our design protocol to include MD simulations that account for water and help evaluate the degree of flexibility of the ligand environment. Controlling polarity and flexibility are essential to adjusting photophysical and photochemical properties and illustrate the importance of using a *de novo* protein host. The design success was validated by solution NMR to ensure tight packing and a unique structure. To evaluate the generality of our design, we engineered the protein to bind two NDI derivatives: one with phenyl (NDI**1**) and the other with alkyl substituents (NDI**2**, Fig. 1B). We also demonstrate their ability to perform photo-triggered intermolecular electron transfer to activate reactive probes in solution for proximity labeling.

RESULTS

Design of NBP1 and MD simulations. Initially we targeted binding of NDI**1** (Fig 1B) due to its ability to form intramolecular charge separate states and the N-phenyl substituents are advantageous for good packing with amino acid sidechains. While the NDI derivatives discussed here are D2 symmetric, they can be derivatized to be asymmetric.[28] Taking advantage of this symmetry offers an excellent starting point by parameterizing D2-symmetric four-helix bundles that can then be expanded to

any NDI scaffold and de-symmetrized during flexible backbone sequence design. In addition to the asymmetric environment provided by the side chains, the twist of the coiled coil can differentiate prochiral centers, providing an approach to modulate the spectroscopic and electronic properties of the NDI in a way that would be difficult to do

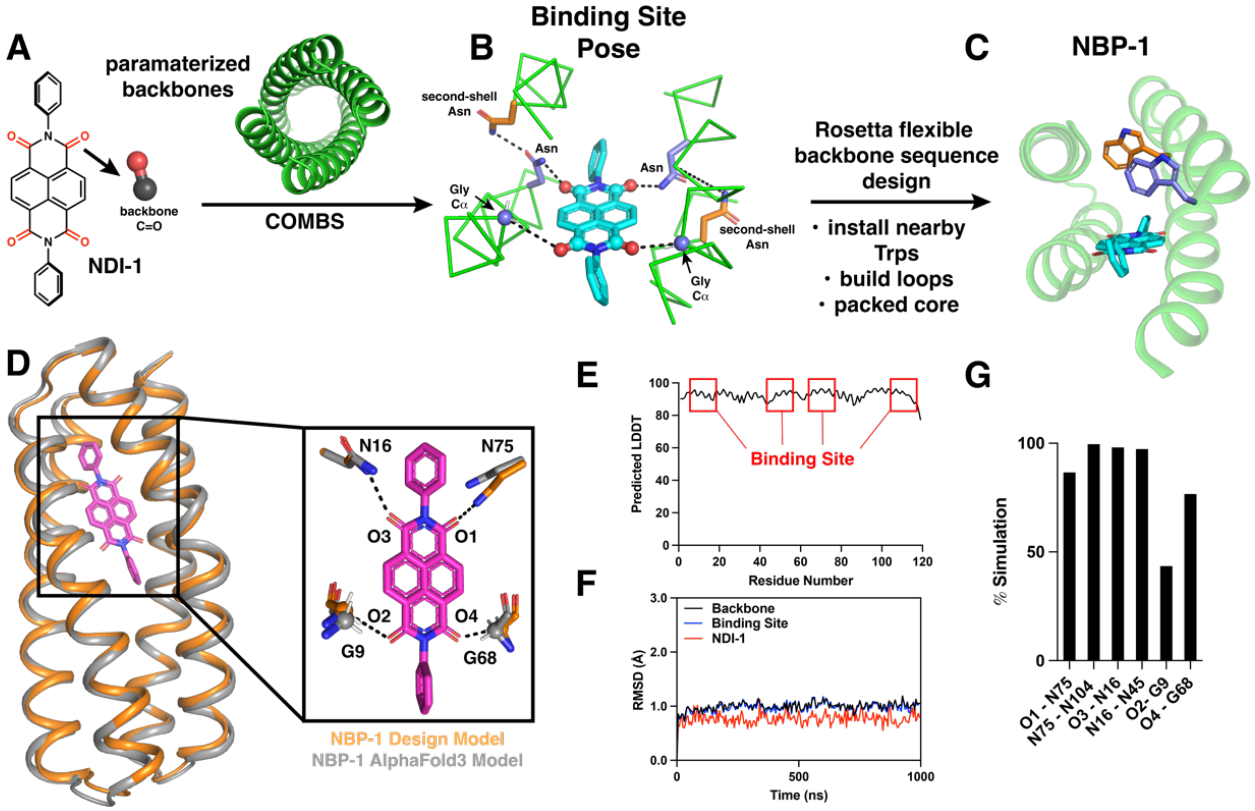

Figure 2. Design process for NBP-1. (**A**) NDI carbonyls are approximated with proteinaceous backbone carbonyl FGs in COMBS. (**B**) A library of parameterized backbones are searched using the COMBS algorithm to find a designable pose that provides H-bonding interactions to the NDI (blue residues) and second-shell H-bonding interactions (orange residues). (**C**) The binding site is constrained and Rosetta flexible backbone sequence design is used to design the remaining sequence. Trp residues placed during the design process at 3.5 Å (blue) and 9.5 Å (orange) as possible electron transfer partners for the NDI. MASTER was used to build loops to make NBP1. (**D**) The AlphaFold3 model agreed with the designed model of NBP-1 with a helical RMSD of 0.81 Å, including excellent prediction of the designed H-bonding sidechains**.** (**E**) Plot of pLDDT from AlphaFold3 showing the strong confidence in the designed protein sequence. Red squares indicate residues within 6 Å of the NDI cofactor. (**F-G**) MD simulations helped inform design stability and dynamics. (F) Averaged RMSD of NBP1-NDI**1** complex over three 1 μs simulations showing extreme stability of the design and impressive RMSD for NDI**1** cofactor within the binding site. Binding site is residues within 10 Å of the cofactor. (**G**) Analysis of designed H-bonding interactions between protein and NDI**1** showing that H-bonds are maintained throughout the simulations.

outside of a protein. Using COMBS, we generated ligand poses on a small library of parametrized helical bundles[29] that included classic as well as C*α*-H H-bonds, illustrating the versatility of this method. The carbonyl groups on the NDI were approximated with amino acid backbone carbonyls[5] (Fig. 2A, see SI), which were used to search for polar interactions to the ligand. We aimed to achieve 2 or more H-bonds to the NDI and were excited to see poses with 4 H-bonds, one to each carbonyl oxygen on the NDI. The most promising pose matched the D2 symmetry of the helical bundle, showing two Asn side chains each donating an H-bond to a carbonyl oxygen, as well as two Gly-C*α* donating H-bonds to the remaining two carbonyl oxygens (Fig. 2B). Gly Cα-H H-bonds, while weaker than prototypical polar H-bonds, are known to be important in ligand binding[30] and enforcing secondary structural motifs,[31] and are thus motifs that should be adequately sampled. In addition, we implemented a recursive version of the COMBS algorithm[4] which allowed us to find vdMs that provide second-shell H-bonding interactions to re-enforce the binding site. With this strategy, we found second-shell Asn residues that donated H-bonds to the carbonyl oxygens of the first-shell Asn donors (Fig 2B). This binding site was constrained during the remaining sequence design (see SI).

Because NDIs possess substantial $^1E^{-/*}$ values, Trp residues were placed at 3.5 Å and 9.5 Å from the NDI (measured closest approach to naphthalene core) as possible electron donors for photoexcited NDI. In addition, there were three Phe residues within 10 Å of the NDI. The full sequence design was accomplished using a custom RosettaScript for flexible backbone sequence design in conjunction with the MASTER algorithm[7, 32] (See SI). The resulting sequence, designated NBP1 has no similarity with any natural proteins (blast *E* value <0.05 against the nonredundant protein database). Two additional designs (NBP2-3) were prepared from the same backbone and had the same

NDI H-bonding interactions but contained varying aromatic residues near the NDI binding site (Fig. S1).

One challenge in ligand binding is accommodating polar residues within the apolar core of a protein. This often leads to instability and increased dynamics of the protein backbone and sidechains. Therefore, we wanted to assess the use of molecular dynamics (MD) as a design tool to help predict successful designs and stable binding site-cofactor interactions. We augmented our design approach with the addition of MD simulations by using models directly from design, rather than from experimental structure; the quality of these designs can thus be readily assessed and subsequently validated with solution NMR spectroscopy (vide infra). To provide insight into the conformational stability of our designs, we conducted 1 µs MD simulations. Overall, the designs showed impressive stability throughout the simulations with average backbone RMSDs all below 1.15Å (Fig 2F, S2). While the protein backbone and binding site in NBP1 were very stable (average RMSD of 0.99 Å and 0.97 Å, respectively), the NDI**1** was exceptionally stable (average RMSD 0.77 Å), illustrating the precisely designed binding site. Moreover, the designed H-bonding interactions remained intact for >85% of the simulation (Fig. 2G). We also observed only three clusters of water molecules near the bound NDI: compared to "free" NDI-**1**, the binding site remains extremely dry (Fig. S3).

For additional confirmation of the structural stability of apo-NBP1, we ran *ab initio* folding predictions in Rosetta[33] and compared the outputs to AlphaFold2[34] and AlphaFold3[35] structure predictions. The *ab initio* calculations showed excellent agreement with our design where the top scoring structure had a backbone RMSD = 0.7 Å (Fig. S4) The AlphaFold2 predictions also confidently predicted the overall structure with an average pLDDT (predicted local distance difference test, a per-residue measure of local confidence) of 88 and all backbone RMSD of 0.86 Å while the AlphaFold3 prediction further improved with an average pLDDT of 88 and all backbone RMSD of 0.81 Å (Fig. 2D-E).

Solution and Structural Characterization. All designed proteins express well in *E. coli* (~20-30 mg/L) and were purified to homogeneity. Spectral titrations indicate that NBP1-3 bound NDI**1** with similar shifts in the absorbance spectrum (Fig. 3A, S5). While all three designs bound the cofactor, NBP**1** had the best solubility properties and was chosen for further characterization. Despite the cofactor's extremely poor water solubility and inherent disposition towards aggregation, NBP**1** tightly binds one equivalent of NDI**1** (Fig. 3B). NDI**1** was added from a DMSO stock solution (binding occurred within the mixing time) and resulted in a shift of the absorption bands at 362 and 382 nm. NDI**1** exhibits a weak, broad absorbance at 388 nm (Fig. 3A-B, red) when added to aqueous buffer due to aggregation.[36] Once isolated within the protein scaffold the bands split into characteristic NDI vibrational modes at 343, 362, and 382 nm with a measured extinction coefficient (ε_{382} = 19,100 $M^{-1}cm^{-1}$) consistent with published values in organic solvent, indicating the NDI**1** is held rigidly in the binding site.[19, 28] Similarly, while NDI**1** is achiral, we expect placement of this synthetic cofactor within the designed rigid binding site to induce chirality. Indeed, the visible CD spectrum of holo-NBP1 shows a clear induced Cotton effect associated with the absorption bands at 362 and 382 nm (Fig. 3C).

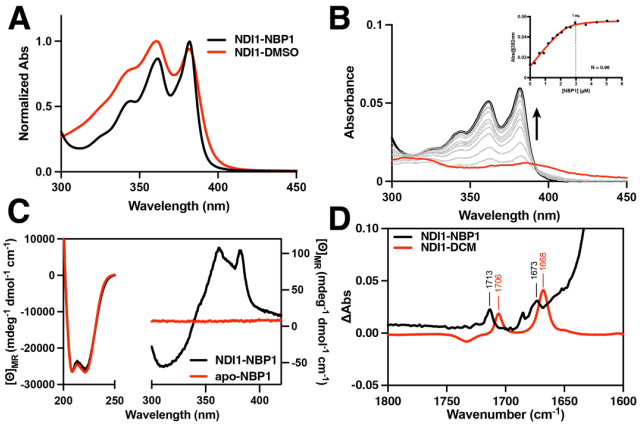

Figure 3. (A) Electronic absorption spectra of holo-NBP1 and free NDI**1** in DMSO showing a shift in the absorbances indicative of binding. (**B**) UV-vis titration of apo-NBP1 into a solution of NDI**1** (3 µM) giving a 1:1 stoichiometry. (**C**) CD spectra showing the helical structure of apo- and NDI**1**-NBP1 and the induced Cotton effect for the NDI absorbances at 362 and 382 nm in the visible region. (**D**) IR difference spectra showing shift in the C=O vibrations between free NDI1 in methylene chloride solvent and NDI1 in NBP1 due to designed H-bonding interactions.

To determine the effect of the designed H-bonding interactions on the C=O vibration of the NDI, we measured solution IR spectra of the NDI**1** and holo-NBP1. We expected to observe the NDI C=O vibrations around 1650 cm^{-1},[37] however they were obscured by the intense amide I stretching frequency from the helical backbone (~1600-1700 cm^{-1}).[38] To address this, we expressed ^{13}C-^{15}N labeled NBP1 to shift the amide I frequency to ~1590 cm^{-1},[39] allowing us to better view the NDI C=O vibrations. In so doing, we saw a shift in the C=O vibrations between free NDI**1** and holo-NBP1 (Fig. 3D). In particular, the band seen at 1706 cm^{-1} for the free NDI was clearly separated from the amide absorption of the protein, and this vibration moved to 1713 cm^{-1} once bound to the protein, indicative of a change in the environment surrounding the cofactor.

To probe the contribution of hydrogen-bonding to the free energy of binding of the cofactor, we determined the dissociation constant for binding of NDI**1** to NBP1 and a mutant in which the first-shell Asn residues were converted to Ala (N16A/N75A, Fig. 4A). NBP1 has two Trp within 10 Å of the cofactor, which is well within the expected Forster distance for energy transfer. Indeed, we observed a quenching of the Trp fluorescence in holo-NBP1. A fluorescence titration of NBP1 with NDI**1** showed a linear increase in the degree of quenching until a stoichiometry of 1:1 is reached, after which no further quenching was observed. This behavior is consistent with relatively tight binding, making it challenging to obtain an accurate dissociation constant from a single titration experiment. To improve accuracy, we conducted a series of four titrations at four different total protein concentrations, demonstrating a classical binding isotherm; a global non-

linear least squares fit of the full set of data provided an apparent dissociation constant of 27 ± 6.7 nM (Fig. 4C). As expected, removal of the two H-bonding Asn residues led to a marked decrease in binding affinity. A titration of

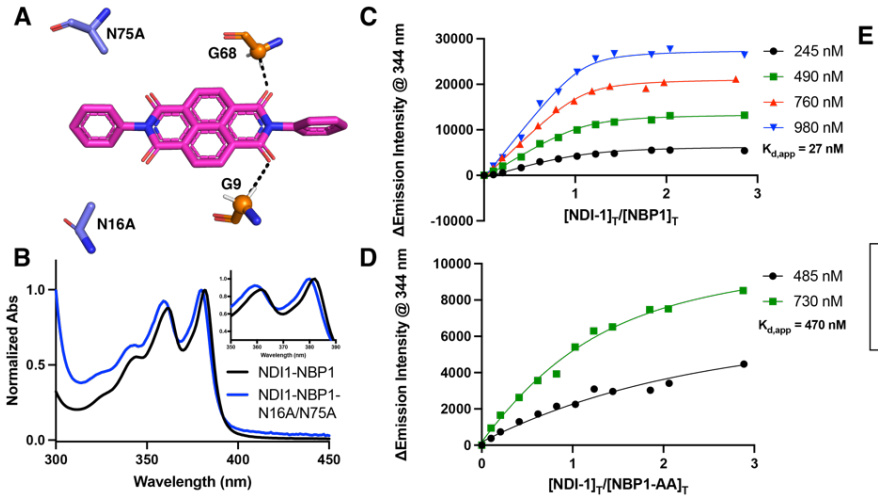

E

	NBP1	NBP1 N15A N75A	ΔΔG (kcal/mol)
$K_{d,app}$ (nM)	27	470	1.7

Figure 4. (A) Model showing Asn to Ala mutations made in NBP1 to disrupt H-bonding interactions. (B) Electronic absorption spectra showing shift in absorbance due to modification of H-bonding environment. Inset: Zoom of absorption maxima. (C-D) Tryptophan fluorescence quenching experiments showing the concentration dependent change in Trp emission at 344 nm. (E) Apparent Kd values from fits of C and D, and calculated ΔΔG value associated with the loss of two H-bonds to NDI-1.

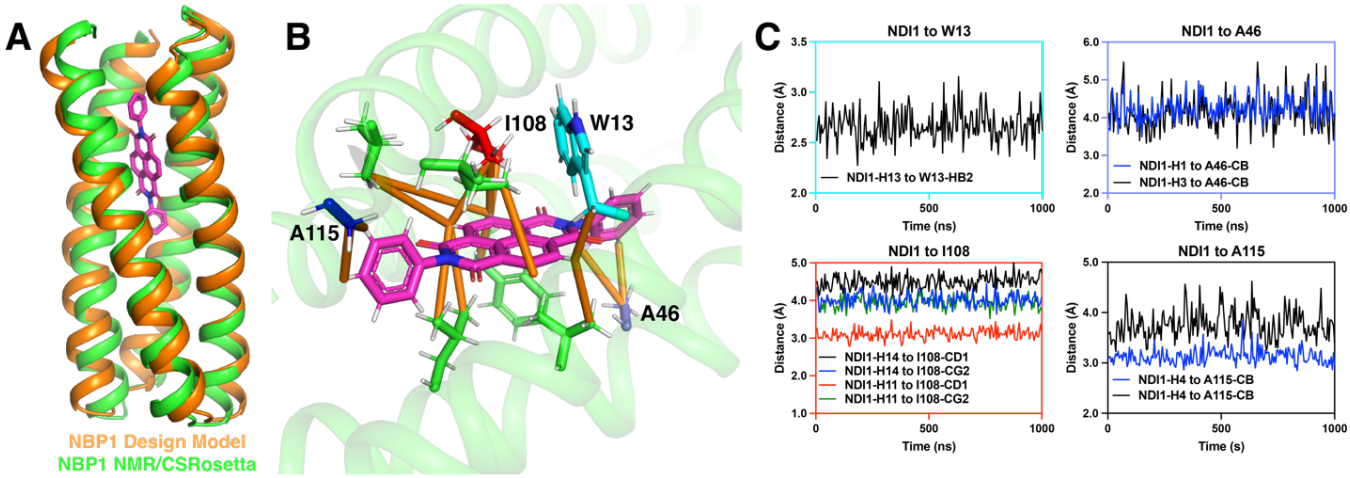

Figure 5. (**A**) Overlay of NDI**1**-NBP1 design model (orange) and calculated NMR structure using CSRosetta (green, PDB 9DM3) showing 0.9 Å helical backbone rmsd. (**B**) 17 protein-NDI NOEs (orange lines) experimentally determine the location and orientation of the NDI-1 cofactor within the binding site of NBP1. (**C**) Analysis of the MD simulations of NDI-1-NBP1 allow us to corroborate measured NOEs. Plots show atom-atom distances over the course of the MD trajectory (see SI for additional detail). All measured NOEs maintained atom-atom distances of <5 Å. Plot boxes are color coded to match their respective residues in (B).

NBP1-N16A/N75A indicated that this mutant had a dissociation constant of 470 nM corresponding to a 1.7 kcal/mole decrease. The change in the H-bonded environment between NBP1 and the double-Asn mutant (N16A/N75A) also leads to a change in the cofactor's electronic absorption spectrum indicating that the electronic structure of NDI is sensitive to the environment (Fig. 4B), consistent with previous studies of the effect of solvent polarity on the spectrum of NDI derivatives.[40]

The use of solution NMR allows us to quickly assess our designs and corroborate the data from MD simulations. Free NDI**1** in d_6-DMSO showed a single ^{1}H signal for the four naphthalene protons, consistent with the D2 symmetry of the molecule (Fig. S6A). However, within the protein, NDI**1** is expected to be desymmetrized, consistent with the asymmetric environment within the protein. Indeed, the chemical shifts show that the NDI protons become non-equivalent within the binding site, providing more evidence for the precise placement of the cofactor, placing the naphthalene protons within different chemical environments (Fig. S6B). In addition, many of the signals from neighboring sidechains are shifted extremely upfield (by as much as 2 ppm) due to the strong ring-current above and below the NDI naphthalene core (Table S1, Fig. S7). These data show that the protein has a well-defined structure that positions the NDI in a single orientation within the binding site.

^{13}C-^{15}N labeled NDI**1**-NBP1 displayed an exceptionally well-resolved ^{1}H-^{15}N HSQC NMR spectra (Fig. S7-S8), congruent with a unique, well-defined structure. The spectral assignments were obtained for 92.3% of the backbone and 69.3% of the sidechain resonances (see SI). These chemical shifts were input into CSRosetta[41-42] to compute a model of its tertiary structure (Fig. 5A). The resulting model (PDB 9DM3) matched the design exceptionally well (helical backbone RMSD 0.9 Å ± 0.18 Å) confirming the unique structure observed by MD. Moreover, we measured 19 nuclear Overhauser effects (NOEs) between NDI**1** and the neighboring sidechains (Fig. 5B, Table S2). Each of these NOEs are in very good agreement with the corresponding proton-proton distances observed in the weighted ensemble of structures computed in our MD simulations (Fig. 5C, S9), which showed that the corresponding protons were within 5 Å. In summary, the unrestrained MD simulations, which were conducted using the design model as a starting structure, were in excellent agreement with the overall backbone structure computed by CSRosetta as well as the detailed contacts reflected in the protein-NDI NOEs (Fig. 5C, Table S2). This illustrates the effectiveness of using MD as a guiding tool during the design process.

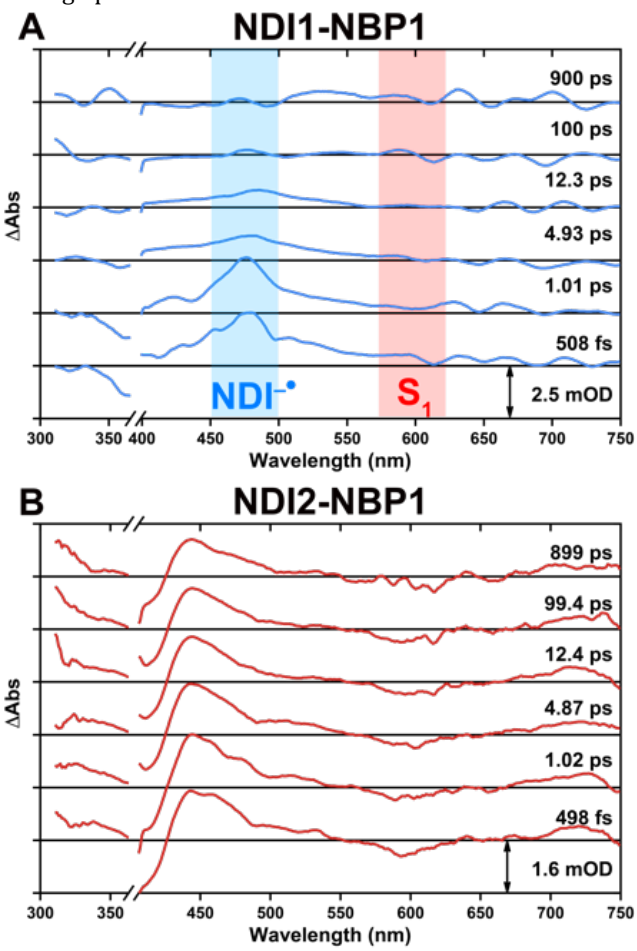

Figure 6. Pump-probe transient dynamics of NBP1 bound to (**A**) NDI-1 displaying intramolecular charge separated species NDI$^{-\bullet}$ (blue) forming as the S1 excited state absorption (red) decays and (**B**) $(C_5H_{11})_2$-NDI. Experimental conditions: Buffer solvent system; ambient temperature; NDI-1-Ph_2, λ_{ex}= 385 nm; NDI-2, λ_{ex}= 385 nm. (**C**) Spectroelectrochemical reduction of free NDI-1 in dichloromethane (blue) overlayed with NDI-2-NBP1 de novo protein in buffer pre-fsta (black) and post-fsTA measurement (red) showing long-lived ground state NDI radical anion photoproduct.

NDI Photophysical Properties. Photophysical characterization of NDI**1**-NBP-1 and NDI**2**-NBP-1 was carried out using pump-probe time-resolved transient optical methods. Electronic excitation (λ_{ex} = 380 nm) of the cofactors in these proteins produces the potent ^{1}NDI* photooxidant. Congruent with data acquired in solution, because the NDI-1 cofactor features imide phenyl (Ph) substituents (**Fig. 1B, S10**), and a ^{1}NDI* state $^{1}E^{-/*}$ potential having sufficient thermodynamic driving force to oxidize unsubstituted arenes,[19] an ultrafast photoinduced intramolecular charge separation (CS) reaction is observed for NDI**1**-NBP1 [$^{1}(Ph)_2$NDI* → $[(Ph)_2]^{\bullet+}$ $(NDI)^{\bullet-}$]. Femtosecond transient absorption (fs-TA) spectroscopic data (**Fig. 6A**) highlight the ^{1}NDI* $S_1 \rightarrow S_n$ transient absorption signal; note that its decay is correlated with the rise of another excited-state absorption (ESA) signal at 480 nm, corresponding to the radical anion NDI$^{\bullet-}$.[43-45] These dynamical data characterize the time constant for photoinduced intramolecular CS in NDI**1**-NBP1 (τ_{CS} < 1 ps). Decay of the NDI$^{\bullet-}$ ESA tracks the dynamics of the intramolecular thermal charge recombination (CR) reaction ($[(Ph)_2]^{\bullet+}$ $(NDI)^{\bullet-}$] → $(Ph)_2$NDI; τ_{CR} ~ 50 ps).

Because NDI**2**-NBP1 features a cofactor in which the NDI N-phenyl substituents are replaced with N-(3-pentyl) groups, a light-triggered intramolecular charge transfer reaction is not possible. Transient absorption spectroscopic data highlight that following optical excitation of NDI**2**-NBP-1, the NDI$^{\bullet-}$ ESA persists over the 500 fs - 1 ns time domain chronicled in **Fig. 6B**. These data are consistent with a photoinduced intermolecular CS reaction that likely involves oxidation of a nearby amino acid (AA) side chain (^{1}(3-pentyl)$_2$NDI* + AA → (3-pentyl)$_2$NDI)$^{\bullet-}$ + AA$^{\bullet+}$) such as Trp, followed by subsequent hole (positive charge) migration that transfers this oxidizing equivalent to a more distant AA site; in the NDI**2**-NBP-1 protein, the timescale of CR exceeds that which may probed in this experiment (> 7 ns).

These NDI**2**-NBP1 photophysical properties indicate its potential utility for photo-triggered protein labeling (**Fig. 7A**).[24, 46-48] Proximity labeling proteomics (PLP) methods are able to spatially label and identify nearby proteins in complex cellular environments by generating reactive intermediates of varying lifetimes .[24] These tools have provided important understanding of protein interactomes within cells.[47] Our NDI binders are ideal for this application, with NDI**2** being particularly promising due to its long-lived excited state, allowing migration of the oxidizing equivalent to the protein surface and beyond. Currently, four types of labeling probes have been used widely in the proximity labeling field[24] including diazirine (P1), aryl-azide (P2), hydrazide (P3), and phenol-biotin (P4) (Figure S11A). [49-52] Diazirine, aryl-azide, and phenol based probes function by formation of reactive carbene, nitrene, and phenol radical species, respectively, via activation by a photocatalyst after irradiation with bio-compatible blue or green light. Alternatively, hydrazide-based probes rely on activation of singlet oxygen (by a

photooxidant) to oxidize surface residues on a protein before subsequent covalent modification by the hydrazide moiety. These probes form intermediates with lifetimes ranging from ns to >100 µs, thus determining how far they can diffuse and spatially differentiate nearby proteins.

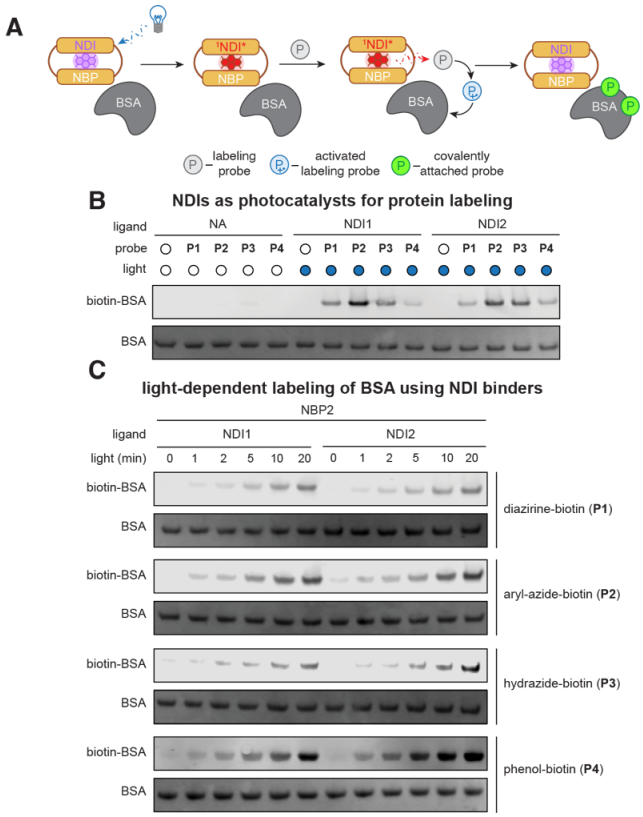

Figure 7: NDI binders perform photo-triggered protein labeling. (**A**) Schematic illustrating NDI binders labeling BSA in solution in a light-dependent manner. (**B**) Western blot of light induced labeling of BSA with free NDI cofactors and (**C**) NBP2 binder with both NDI cofactors showing their ability to activate and label BSA with four labeling probes.

To test whether our designed NDI-binders were competent for this type of labeling strategy, we first confirmed via Western blot that both free-NDI compounds (NDI**1** and NDI**2**) can trigger protein labeling on purified protein upon illumination of LED light (**Fig. 7B**). Given that P2 (the aryl-azide probe) demonstrated the highest level of labeling on bovine serum albumin (BSA) with free NDI cofactors, we therefore used P2 to screen NDI binders for labeling efficiency (Fig. S11C). After confirming that no significant change in absorption spectrum was observed after irradiation of all the binders (Figure S11B), we screened three NDI binders (NBP1, NBP2, and NBP3) with both NDI cofactors for self-labeling (Figure S11C). We found that NBP2 demonstrated the best self-labeling efficiency compared with NBP1 and NBP3, with slightly enhanced performance for NDI**2** compared with NDI**1**. This was not surprising given the NDI**1** proclivity for *intra*molecular charge transfer, which is avoided in the alkyl-NDI derivative. Since NBP2 exhibited the best performance, we then tested NDI**1**-NBP2 and NDI**2**-NBP2 to perform photolabeling on BSA using P1-P4 to gauge the ability to activate a range of probes. By performing time-dependent labeling reactions, we observed significant accumulation of biotinylated BSA with all probes (Figure 7C). BSA labeling was also light-dependent, reaching a plateau with 10-20 min of irradiation. These results demonstrate that NDI binders are capable of intermolecular electron transfer to labeling probes in solution and can label proteins successfully *in vitro*. Moreover, the modulation in activity between protein scaffold and NDI-derivative suggests this could be a good platform for further development of enhanced protein labeling tools.

DISCUSSION

The ability to bind diverse ligands with high affinity opens up a world of function beyond binding, including catalysis, photophysics, and photochemistry. In this study we augmented our protein design methods with MD to build polar binding sites for abiological NDI cofactors. Using COMBS, we built a binding site that included four H-bonding interactions to the NDI (traditional H-bonds, as well as Gly Ca H-bonds) and designed three proteins that all bound the desired cofactor, including one that bound with ~30 nM affinity. This speaks to the power of our design process where we can design successful binders without the need for high-throughput experimental screening or evolution. In addition, the use of solution NMR allowed us to readily assess the success of our designs. We identified a substantial number of NDI**1**-NBP1 NOEs which were corroborated with our MD simulations and showed that the calculated backbone structure of holo-NBP1 matched the design with 0.9 Å RMSD. While we used 1µs MD simulations to assess solution dynamics and hydration of the cofactor, 200 ns simulations are likely sufficient for rapid assessment directly from design models. This also allows for explicit consideration of water molecules, which are important in ligand binding as well as controlling the polarity and, therefore, photophysical properties of bound molecules.

NDIs are powerful photooxidants with tunable photophysical properties. Using fs-TA, we showed that NDI-1 bound to NBP1 was able to form the potent ^{1}NDI* photooxidant and undergo photoinduced *intra*molecular CS, forming a short lived (<1 ps) charge-separated state [^{1}(Ph)$_2$NDI* → [(Ph)$_2$]$^{\bullet+}$(NDI)$^{\bullet-}$]. NBP1 also included oxidizable Trp residues in close proximity (3.5 and 9.5 Å), poised to undergo *inter*molecular electron transfer with a photoactivated NDI. Therefore, we employed the synthetic tunability of the NDI scaffold and replaced the N-phenyl groups with N-3-pentyl substituents (NDI**2**) to avoid self-oxidation. As a result, we observed a photoinduced long-lived (>7 ns) CS resulting from intermolecular electron transfer between NDI and, likely, an oxidizable AA residue (^{1}(3-pentyl)$_2$NDI* + AA → (3-pentyl)$_2$NDI)$^{\bullet-}$ + AA$^{\bullet+}$). Furthermore, to illustrate the potential for this system we showed the ability of the designed NDI binders to activate four labeling probes in a light-dependent manner and label BSA *in vitro*. This platform shows great potential to harness and tune the photophysics of bound NDIs by leveraging protein design with synthetic modification of NDI for use in photochemical applications.

ASSOCIATED CONTENT

Supporting Information

The Supporting Information is available free of charge on the ACS Publications website.

Methods for protein design, protein expression, NMR, MD, spectroscopy, and photolabeling experiments, along with Figures S1-S13, Tables S1-S2, and Scheme S1 (PDF)

Accession Code. NMR Chemical Shift information has been deposited in Biologial Magnetic Resonance Data Bank (BMRB) with accession number 52600. CSRosetta structure has been deposited in the Protein Data Bank with accession code 9DM3.

AUTHOR INFORMATION

Corresponding Author

*William F. DeGrado: william.degrado@ucsf.edu; Michael J. Therien: michael.therien@duke.edu; James A. Wells: jim.wells@ucsf.edu; Yibing Wu: yibing.wu@ucsf.edu

Present Addresses

†Department of Chemistry, University of California, Riverside, California 92521, United States

†† Department of Chemistry, Duke Kunshan University, Kunshan, Jiangsu Province, 215316, China

ACKNOWLEDGMENT

The authors acknowledge the National Science Foundation (CHE-2109020; NSF CHE-2108660), the Keck Foundation, and National Institute of Health (GM R35 122603, 1R01CA248323-01; 5K99GM143529-02) for supporting this work. MJT is indebted to the United States Department of Energy (DE-SC0001517) and the United States Air Force Office of Scientific Research (FA9550-20-1-0121) for research infrastructure enabling transient dynamical spectroscopic experiments.

REFERENCES

1. Huang, P. S.; Boyken, S. E.; Baker, D., The coming of age of de novo protein design. *Nature* **2016,** *537*, 320-327
2. Vega-Penaloza, A.; Mateos, J.; Companyo, X.; Escudero-Casao, M.; Dell'Amico, L., A Rational Approach to Organo-Photocatalysis: Novel Designs and Structure-Property Relationships. *Angew. Chem., Int. Ed. Engl.* **2021,** *60*, 1082-1097
3. Millet, A.; Cesana, P. T.; Sedillo, K.; Bird, M. J.; Schlau-Cohen, G. S.; Doyle, A. G.; MacMillan, D. W. C.; Scholes, G. D., Bioinspired Supercharging of Photoredox Catalysis for Applications in Energy and Chemical Manufacturing. *Acc. Chem. Res.* **2022,** *55*, 1423-1434
4. Lu, L.; Gou, X.; Tan, S. K.; Mann, S. I.; Yang, H.; Zhong, X.; Gazgalis, D.; Valdiviezo, J.; Jo, H.; Wu, Y.; Diolaiti, M. E.; Ashworth, A.; Polizzi, N. F.; DeGrado, W. F., De novo design of drug-binding proteins with predictable binding energy and specificity. *Science* **2024,** *384*, 106-112
5. Polizzi, N. F.; DeGrado, W. F., A defined structural unit enables de novo design of small-molecule-binding proteins. *Science* **2020,** *369*, 1227-1233.PMC7526616
6. Polizzi, N. F.; Wu, Y.; Lemmin, T.; Maxwell, A. M.; Zhang, S.-Q.; Rawson, J.; Beratan, D. N.; Therien, M. J.; DeGrado, W. F., De novo design of a hyperstable non-natural protein–ligand complex with sub-Å accuracy. *Nat. Chem.* **2017,** *9*, 1157-1164
7. Mann, S. I.; Nayak, A.; Gassner, G. T.; Therien, M. J.; DeGrado, W. F., De Novo Design, Solution Characterization, and Crystallographic Structure of an Abiological Mn-Porphyrin-Binding Protein Capable of Stabilizing a Mn(V) Species. *J. Am. Chem. Soc.* **2021,** *143*, 252-259.PMC8006777
8. Dauparas, J.; Lee, G. R.; Pecoraro, R.; An, L.; Anishchenko, I.; Glasscock, C.; Baker, D., Atomic context-conditioned protein sequence design using LigandMPNN. *bioRxiv* **2023**, 2023.2012.2022.573103
9. Krishna, R.; Wang, J.; Ahern, W.; Sturmfels, P.; Venkatesh, P.; Kalvet, I.; Lee, G. R.; Morey-Burrows, F. S.; Anishchenko, I.; Humphreys, I. R.; McHugh, R.; Vafeados, D.; Li, X.; Sutherland, G. A.; Hitchcock, A.; Hunter, C. N.; Kang, A.; Brackenbrough, E.; Bera, A. K.; Baek, M.; DiMaio, F.; Baker, D., Generalized biomolecular modeling and design with RoseTTAFold All-Atom. *Science* **2024,** *384*, eadl2528
10. Tinberg, C. E.; Khare, S. D.; Dou, J.; Doyle, L.; Nelson, J. W.; Schena, A.; Jankowski, W.; Kalodimos, C. G.; Johnsson, K.; Stoddard, B. L.; Baker, D., Computational design of ligand-binding proteins with high affinity and selectivity. *Nature* **2013,** *501*, 212-216
11. Dou, J.; Vorobieva, A. A.; Sheffler, W.; Doyle, L. A.; Park, H.; Bick, M. J.; Mao, B.; Foight, G. W.; Lee, M. Y.; Gagnon, L. A.; Carter, L.; Sankaran, B.; Ovchinnikov, S.; Marcos, E.; Huang, P. S.; Vaughan, J. C.; Stoddard, B. L.; Baker, D., De novo design of a fluorescence-activating beta-barrel. *Nature* **2018,** *561*, 485-491.PMC6275156
12. Dou, J.; Doyle, L.; Jr Greisen, P.; Schena, A.; Park, H.; Johnsson, K.; Stoddard, B. L.; Baker, D., Sampling and energy evaluation challenges in ligand binding protein design. *Protein. Sci.* **2017,** *26*, 2426-2437.PMC5699494
13. Bhosale, S. V.; Al Kobaisi, M.; Jadhav, R. W.; Morajkar, P. P.; Jones, L. A.; George, S., Naphthalene diimides: perspectives and promise. *Chem. Soc. Rev.* **2021,** *50*, 9845-9998
14. Kobaisi, M. A.; Bhosale, S. V.; Latham, K.; Raynor, A. M.; Bhosale, S. V., Functional Naphthalene Diimides: Synthesis, Properties, and Applications. *Chem. Rev.* **2016,** *116*, 11685-11796
15. Jameel, M. A.; Yang, T. C.-J.; Wilson, G. J.; Evans, R. A.; Gupta, A.; Langford, S. J., Naphthalene diimide-based electron transport materials for perovskite solar cells. *J. Mat. Chem. A* **2021,** *9*, 27170-27192
16. Collie, G. W.; Promontorio, R.; Hampel, S. M.; Micco, M.; Neidle, S.; Parkinson, G. N., Structural basis for telomeric G-quadruplex targeting by naphthalene diimide ligands. *J. Am. Chem. Soc.* **2012,** *134*, 2723-2731
17. Redmore, N. P.; Rubtsov, I. V.; Therien, M. J., Synthesis, electronic structure, and electron transfer dynamics of (Aryl)ethynyl-bridged donor-acceptor systems. *J. Am. Chem. Soc.* **2003,** *125*, 8769-8778
18. Xu, W.-J.; Huang, B.-X.; Li, G.; Yang, F.; Lin, W.; Gu, J.-X.; Deng, H.-G.; Gu, Z.-G.; Jin, H.-G., Donor–Acceptor Mixed-Naphthalene Diimide-Porphyrin MOF for Boosting Photocatalytic Oxidative Coupling of Amines. *ACS Catalysis* **2023,** *13*, 5723-5732
19. Ganesan, P.; Baggerman, J.; Zhang, H.; Sudholter, E. J.; Zuilhof, H., Femtosecond time-resolved photophysics of 1,4,5,8-naphthalene diimides. *J. Phys. Chem. A* **2007,** *111*, 6151-6156
20. Christgen, S. L.; Becker, S. M.; Becker, D. F., Methods for determining the reduction potentials of flavin enzymes. *Method. Enzymol.* **2019,** *620*, 1-25
21. Caby, S.; Bouchet, L. M.; Argüello, J. E.; Rossi, R. A.; Bardagi, J. I., Excitation of Radical Anions of Naphthalene Diimides in Consecutive- and Electro-Photocatalysis**. *ChemCatChem* **2021,** *13*, 3001-3009
22. Insuasty, A.; Maniam, S.; Langford, S. J., Recent Advances in the Core-Annulation of Naphthalene Diimides. *Chem. Eur. J.* **2019,** *25*, 7058-7073
23. Suraru, S. L.; Wurthner, F., Strategies for the synthesis of functional naphthalene diimides. *Angew. Chem. Int. Ed.* **2014,** *53*, 7428-7448

24. Lin, Z.; Schaefer, K.; Lui, I.; Yao, Z.; Fossati, A.; Swaney, D. L.; Palar, A.; Sali, A.; Wells, J. A., Multiscale photocatalytic proximity labeling reveals cell surface neighbors on and between cells. *Science* **2024,** *385*, eadl5763

25. Polizzi, N. F.; Eibling, M. J.; Perez-Aguilar, J. M.; Rawson, J.; Lanci, C. J.; Fry, H. C.; Beratan, D. N.; Saven, J. G.; Therien, M. J., Photoinduced Electron Transfer Elicits a Change in the Static Dielectric Constant of a de Novo Designed Protein. *J. Am. Chem. Soc.* **2016,** *138*, 2130-2133.PMC5049705

26. Fujitsuka, M.; Kim, S. S.; Lu, C.; Tojo, S.; Majima, T., Intermolecular and Intramolecular Electron Transfer Processes from Excited Naphthalene Diimide Radical Anions. *J. Phys. Chem. B* **2015,** *119*, 7275-7282

27. Zieschang, F.; Schreck, M. H.; Schmiedel, A.; Holzapfel, M.; Klein, J. H.; Walter, C.; Engels, B.; Lambert, C., Photoinduced Electron Transfer Dynamics in Triarylamine–Naphthalene Diimide Cascades. *J. Phys. Chem. C* **2014,** *118*, 27698-27714

28. Sakai, N.; Mareda, J.; Vauthey, E.; Matile, S., Core-substituted naphthalenediimides. *Chem. Commun.* **2010,** *46*, 4225-4237

29. Grigoryan, G.; Degrado, W. F., Probing designability via a generalized model of helical bundle geometry. *J. Mol. Biol.* **2011,** *405*, 1079-1100.PMC3052747

30. Sarkhel, S.; Desiraju, G. R., N-H...O, O-H...O, and C-H...O hydrogen bonds in protein-ligand complexes: strong and weak interactions in molecular recognition. *Proteins* **2004,** *54*, 247-259

31. Kleiger, G.; Eisenberg, D., GXXXG and GXXXA motifs stabilize FAD and NAD(P)-binding Rossmann folds through C(alpha)-H... O hydrogen bonds and van der waals interactions. *J. Mol. Biol.* **2002,** *323*, 69-76

32. Zhou, J.; Grigoryan, G., Rapid search for tertiary fragments reveals protein sequence-structure relationships. *Protein Sci.* **2015,** *24*, 508-524.PMC4380982

33. Bradley, P.; Misura, K. M.; Baker, D., Toward high-resolution de novo structure prediction for small proteins. *Science* **2005,** *309*, 1868-1871

34. Jumper, J.; Evans, R.; Pritzel, A.; Green, T.; Figurnov, M.; Ronneberger, O.; Tunyasuvunakool, K.; Bates, R.; Zidek, A.; Potapenko, A.; Bridgland, A.; Meyer, C.; Kohl, S. A. A.; Ballard, A. J.; Cowie, A.; Romera-Paredes, B.; Nikolov, S.; Jain, R.; Adler, J.; Back, T.; Petersen, S.; Reiman, D.; Clancy, E.; Zielinski, M.; Steinegger, M.; Pacholska, M.; Berghammer, T.; Bodenstein, S.; Silver, D.; Vinyals, O.; Senior, A. W.; Kavukcuoglu, K.; Kohli, P.; Hassabis, D., Highly accurate protein structure prediction with AlphaFold. *Nature* **2021,** *596*, 583-589.PMC8371605

35. Abramson, J.; Adler, J.; Dunger, J.; Evans, R.; Green, T.; Pritzel, A.; Ronneberger, O.; Willmore, L.; Ballard, A. J.; Bambrick, J.; Bodenstein, S. W.; Evans, D. A.; Hung, C. C.; O'Neill, M.; Reiman, D.; Tunyasuvunakool, K.; Wu, Z.; Zemgulyte, A.; Arvaniti, E.; Beattie, C.; Bertolli, O.; Bridgland, A.; Cherepanov, A.; Congreve, M.; Cowen-Rivers, A. I.; Cowie, A.; Figurnov, M.; Fuchs, F. B.; Gladman, H.; Jain, R.; Khan, Y. A.; Low, C. M. R.; Perlin, K.; Potapenko, A.; Savy, P.; Singh, S.; Stecula, A.; Thillaisundaram, A.; Tong, C.; Yakneen, S.; Zhong, E. D.; Zielinski, M.; Zidek, A.; Bapst, V.; Kohli, P.; Jaderberg, M.; Hassabis, D.; Jumper, J. M., Accurate structure prediction of biomolecular interactions with AlphaFold 3. *Nature* **2024**,

36. Balakrishnan, K.; Datar, A.; Naddo, T.; Huang, J.; Oitker, R.; Yen, M.; Zhao, J.; Zang, L., Effect of side-chain substituents on self-assembly of perylene diimide molecules: morphology control. *J. Am. Chem. Soc.* **2006,** *128*, 7390-7398

37. Wang, L.; Goodloe, G. W.; Stallman, B. J.; Cammarata, V., Synthesis, Electrooxidation, and Characterization of Bis(diphenylamine)naphthalene Diimide. *Chem. Mater.* **1996,** *8*, 1175-1181

38. Ganim, Z.; Chung, H. S.; Smith, A. W.; Deflores, L. P.; Jones, K. C.; Tokmakoff, A., Amide I two-dimensional infrared spectroscopy of proteins. *Acc. Chem. Res.* **2008,** *41*, 432-441

39. Zhang, M.; Fabian, H.; Mantsch, H. H.; Vogel, H. J., Isotope-edited Fourier transform infrared spectroscopy studies of calmodulin's interaction with its target peptides. *Biochemistry* **1994,** *33*, 10883-10888

40. Doria, F.; Gallati, C. M.; Freccero, M., Hydrosoluble and solvatochromic naphthalene diimides with NIR absorption. *Org. Biomol. Chem.* **2013,** *11*, 7838-7842

41. Mao, B.; Tejero, R.; Baker, D.; Montelione, G. T., Protein NMR structures refined with Rosetta have higher accuracy relative to corresponding X-ray crystal structures. *J. Am. Chem. Soc.* **2014,** *136*, 1893-1906.PMC4129517

42. Leman, J. K.; Weitzner, B. D.; Lewis, S. M.; Adolf-Bryfogle, J.; Alam, N.; Alford, R. F.; Aprahamian, M.; Baker, D.; Barlow, K. A.; Barth, P.; Basanta, B.; Bender, B. J.; Blacklock, K.; Bonet, J.; Boyken, S. E.; Bradley, P.; Bystroff, C.; Conway, P.; Cooper, S.; Correia, B. E.; Coventry, B.; Das, R.; De Jong, R. M.; DiMaio, F.; Dsilva, L.; Dunbrack, R.; Ford, A. S.; Frenz, B.; Fu, D. Y.; Geniesse, C.; Goldschmidt, L.; Gowthaman, R.; Gray, J. J.; Gront, D.; Guffy, S.; Horowitz, S.; Huang, P. S.; Huber, T.; Jacobs, T. M.; Jeliazkov, J. R.; Johnson, D. K.; Kappel, K.; Karanicolas, J.; Khakzad, H.; Khar, K. R.; Khare, S. D.; Khatib, F.; Khramushin, A.; King, I. C.; Kleffner, R.; Koepnick, B.; Kortemme, T.; Kuenze, G.; Kuhlman, B.; Kuroda, D.; Labonte, J. W.; Lai, J. K.; Lapidoth, G.; Leaver-Fay, A.; Lindert, S.; Linsky, T.; London, N.; Lubin, J. H.; Lyskov, S.; Maguire, J.; Malmstrom, L.; Marcos, E.; Marcu, O.; Marze, N. A.; Meiler, J.; Moretti, R.; Mulligan, V. K.; Nerli, S.; Norn, C.; O'Conchuir, S.; Ollikainen, N.; Ovchinnikov, S.; Pacella, M. S.; Pan, X.; Park, H.; Pavlovicz, R. E.; Pethe, M.; Pierce, B. G.; Pilla, K. B.; Raveh, B.; Renfrew, P. D.; Burman, S. S. R.; Rubenstein, A.; Sauer, M. F.; Scheck, A.; Schief, W.; Schueler-Furman, O.; Sedan, Y.; Sevy, A. M.; Sgourakis, N. G.; Shi, L.; Siegel, J. B.; Silva, D. A.; Smith, S.; Song, Y.; Stein, A.; Szegedy, M.; Teets, F. D.; Thyme, S. B.; Wang, R. Y.; Watkins, A.; Zimmerman, L.; Bonneau, R., Macromolecular modeling and design in Rosetta: recent methods and frameworks. *Nat. Methods.* **2020,** *17*, 665-680

43. La Porte, N. T.; Martinez, J. F.; Hedstrom, S.; Rudshteyn, B.; Phelan, B. T.; Mauck, C. M.; Young, R. M.; Batista, V. S.; Wasielewski, M. R., Photoinduced electron transfer from rylenediimide radical anions and dianions to Re(bpy)(CO)(3) using red and near-infrared light. *Chem. Sci.* **2017,** *8*, 3821-3831.PMC5436599

44. Chopin, S.; Chaignon, F.; Blart, E.; Odobel, F., Syntheses and properties of core-substituted naphthalene bisimides with aryl ethynyl or cyano groups. *J. Mat. Chem.* **2007,** *17*,

45. Roznyatovskiy, V. V.; Gardner, D. M.; Eaton, S. W.; Wasielewski, M. R., Radical anions of trifluoromethylated perylene and naphthalene imide and diimide electron acceptors. *Org. Lett.* **2014,** *16*, 696-699

46. Qin, W.; Cho, K. F.; Cavanagh, P. E.; Ting, A. Y., Deciphering molecular interactions by proximity labeling. *Nat. Methods* **2021,** *18*, 133-143.PMC10548357

47. Seath, C. P.; Trowbridge, A. D.; Muir, T. W.; MacMillan, D. W. C., Reactive intermediates for interactome mapping. *Chem. Soc. Rev.* **2021,** *50*, 2911-2926

48. To, T. L.; Medzihradszky, K. F.; Burlingame, A. L.; DeGrado, W. F.; Jo, H.; Shu, X., Photoactivatable protein labeling by singlet oxygen mediated reactions. *Bioorg. Med. Chem. Lett.* **2016,** *26*, 3359-3363.PMC4903891

49. Geri, J. B.; Oakley, J. V.; Reyes-Robles, T.; Wang, T.; McCarver, S. J.; White, C. H.; Rodriguez-Rivera, F. P.; Parker, D. L., Jr.; Hett, E. C.; Fadeyi, O. O.; Oslund, R. C.; MacMillan, D. W. C., Microenvironment mapping via Dexter energy transfer on immune cells. *Science* **2020,** *367*, 1091-1097.PMC7336666

50. Oakley, J. V.; Buksh, B. F.; Fernandez, D. F.; Oblinsky, D. G.; Seath, C. P.; Geri, J. B.; Scholes, G. D.; MacMillan, D. W. C., Radius measurement via super-resolution microscopy enables the development of a variable radii proximity labeling platform. *Proc. Natl. Acad. Sci.* **2022,** *119*, e2203027119.PMC9371666

51. Muller, M.; Grabnitz, F.; Barandun, N.; Shen, Y.; Wendt, F.; Steiner, S. N.; Severin, Y.; Vetterli, S. U.; Mondal, M.; Prudent, J. R.; Hofmann, R.; van Oostrum, M.; Sarott, R. C.; Nesvizhskii, A. I.; Carreira, E. M.; Bode, J. W.; Snijder, B.; Robinson, J. A.; Loessner, M. J.; Oxenius, A.; Wollscheid, B., Light-mediated discovery of surfaceome nanoscale organization and intercellular receptor interaction networks. *Nat. Commun.* **2021,** *12*, 7036.PMC8639842

52. Qin, W.; Cheah, J. S.; Xu, C.; Messing, J.; Freibaum, B. D.; Boeynaems, S.; Taylor, J. P.; Udeshi, N. D.; Carr, S. A.; Ting, A. Y., Dynamic mapping of proteome trafficking within and between living cells by TransitID. *Cell* **2023,** *186*, 3307-3324 e3330.PMC10527209